

# Study on Hardening Parameters and Elastoplastic Constitutive Model of Rockfill Materials

Zhitao Zhang<sup>1,2,3</sup>, Enyue Ji<sup>1,2\*</sup>, Zhongzhi Fu<sup>1,2</sup>, Shengshui Chen<sup>1,2</sup>, Zheng Li<sup>1,3</sup>

<sup>1</sup> Key Laboratory of Reservoir and Dam Safety Ministry of Water Resources, Nanjing 210029, China

<sup>2</sup> Geotechnical Engineering Department, Nanjing Hydraulic Research Institute, Nanjing 210024, China

<sup>3</sup> Dam Safety Management Center of the Ministry of Water Resources, Nanjing 210029, China

\* Corresponding author, e-mail: [eyji@nhri.cn](mailto:eyji@nhri.cn)

Received: 09 July 2025, Accepted: 27 March 2026, Published online: 27 April 2026

## Abstract

An elastoplastic constitutive model is proposed to account for stress loading effects based on triaxial test results of granite rockfill materials. The model utilizes an extended yield function to flexibly control the yield surface shape, distinguishing between loading, unloading, and neutral loading conditions. A non-associated flow rule is implemented, incorporating a critical dilatancy stress ratio into the dilatancy equation to capture particle breakage behavior. The model primarily focuses on the formulation of a stress-path-independent hardening parameter based on the dilatancy equation. A total of 12 model parameters are introduced, all of which can be determined from two conventional laboratory geotechnical tests. Finally, the validity of the proposed model is verified through triaxial test results of various rockfill materials.

## Keywords

constitutive model, dilatancy equation, hardening parameter, rockfill material

## 1 Introduction

To date, several earth-rockfill dams under construction or planned worldwide have reached heights of 300 meters or more [1–3]. Accurately predicting the deformation magnitude and its distribution pattern of these ultra-high dams is essential for deformation control [4–6]. Over the years, finite element numerical simulation methods based on coarse-grained soil constitutive models have become the primary means for stress-deformation prediction [7–10]. However, deformation predictions using existing coarse-grained soil constitutive models often exhibit significant discrepancies with measured data [11]. Therefore, further research into the elastoplastic constitutive models for coarse-grained soils is needed.

An elastoplastic constitutive model consists of three fundamental components: the yield function, the plastic potential function (or dilation equation), and the hardening function. These elements respectively define the onset, direction, and evolution of plastic strain. Based on these functions, the elastoplastic stiffness matrix can be derived to calculate the stress–strain relationship of the material. Clearly, determining the form of the hardening parameters is one of the key aspects in developing elastoplastic

constitutive models for coarse-grained soils [12, 13]. The development of plastic strain is the fundamental cause of soil hardening and serves as a critical factor in defining the hardening parameters. Previous studies [14–17] have shown that using plastic volumetric strain, plastic shear strain, or a combination of these factors ( $f(\varepsilon_v^p, \varepsilon_s^p)$ ) as hardening parameters is a common approach.

The Modified Cam-Clay (MCC) model is widely regarded as one of the most representative elastoplastic models for soils. The original Cam-Clay and Modified Cam-Clay models were proposed by Roscoe et al. [18] from the University of Cambridge and by Hsieh et al. [19] to characterize the stress–strain behavior of normally consolidated clays, which exhibit monotonic coupled hardening. In the modified Cambridge model, the hardening parameter  $H$  is a function of plastic volumetric strain ( $\varepsilon_v^p$ ), meaning that in the  $p$ – $q$  space, the profile of  $\varepsilon_{vp}$  is elliptical, with larger elliptical yield surfaces corresponding to higher plastic volumetric strain ( $\varepsilon_v^p$ ). While this characteristic is suitable for normally consolidated clays, it does not apply to coarse-grained materials like rockfill, as shear-induced dilatancy may occur [20–22]. That is, if plastic

volumetric strain is solely used as a hardening parameter, it will not increase monotonically during shear, which contradicts the continuous expansion of the yield surface.

For soils exhibiting complex hardening behavior and non-monotonic volumetric-strain coupling, a central challenge in elastoplastic theory has been the formulation of incremental functions related to volumetric strain to accurately capture the hardening process. Experimental observations have shown that overconsolidated clays and dense sands typically exhibit non-monotonic coupled hardening behavior. Consequently, extensive research has been conducted to characterize their stress-strain responses. Dafalias [23] introduced a state parameter defined by the distance from the current stress point to the bounding surface to quantify the plastic stiffness and its degradation rate in overconsolidated clays. Hashiguchi [24], building on the MCC model, proposed the concept of a subloading surface to describe the yielding behavior during loading. Whittle and Kavvas [25] suggested that the yield surface gradually rotates during loading to account for stress-induced anisotropy.

Due to the inability of the MCC model to accurately capture the hardening behavior of soils with non-monotonic coupled hardening, Yao et al. [26, 27] introduced a stress-path-related factor and derived a hardening parameter that is independent of the stress path for geomaterials. The derivation employed an associated flow rule, with dilatant materials (such as sand) used in the analysis along the constant  $p$  path. Although both rockfill and sand are granular materials, the mechanical differences between them cannot be entirely overlooked. Additionally, for elastoplastic modeling of rockfill, the form of the dilatancy equation is typically specified, making the use of a non-associated flow rule more suitable [28, 29].

This study aims to develop an elastoplastic constitutive model that captures the stress-strain behavior of rockfill materials under loading. The model is derived by specifying a yield function, a stress-dependent dilatancy equation, and a hardening rule. A key feature of the model is the adoption of a non-associated flow rule, leading to the construction of a more generalized, stress-path-independent hardening parameter for rockfill materials. The model has been validated using typical experimental data and can provide scientific support for deformation prediction and control in ultra-high earth-rock dams. Throughout the paper, compressive stress and strain are defined as positive values, and all positive stresses are considered effective stresses. For simplicity, commonly used primes are omitted.

## 2 Stress loading elastoplastic constitutive model

### 2.1 Elastic behavior

Based on previous experimental observations [6], the stress-strain relationship of the elastic behavior of rockfill materials is given by combining the bulk modulus  $K^e$  and the shear modulus  $G^e$ :

$$\begin{cases} K^e = k_v^e p_a \left(\frac{p}{p_a}\right)^m \\ G^e = k_s^e p_a \left(\frac{p}{p_a}\right)^n \end{cases} \quad (1)$$

In Eq. (1), in order to maintain the consistency of dimension, the standard atmospheric pressure ( $p_a \approx 100$  kPa) is introduced, and  $k_v^e$ ,  $k_s^e$ ,  $m$  and  $n$  are four material parameters.

### 2.2 Yield function

In elastic-plastic theory, the yield function is generally defined by a stress invariant and a certain form of hardening parameter to distinguish between loading, unloading and neutral loading conditions. In this study, the yield function used is in the following form:

$$f(p, q, H) = (c_v - c_v^e) \left(\frac{p}{p_a}\right)^{m_v} \left(1 + \frac{m_v}{2 - m_v} \frac{q^2}{M^2 p^2}\right) - H = 0. \quad (2)$$

The partial derivatives of the yield function  $f(p, q, H)$  with respect to the mean normal stress  $p$  and the generalized shear stress  $q$  are given by

$$\begin{cases} \frac{\partial f}{\partial p} = \frac{m_v}{p} \left(\frac{p}{p_a}\right)^{m_v} \left(1 - \frac{\eta^2}{M^2}\right) \\ \frac{\partial f}{\partial q} = \frac{m_v}{(2 - m_v)p} \left(\frac{p}{p_a}\right)^{m_v} \frac{2\eta}{M^2} \end{cases} \quad (3)$$

In Eq. (3),  $c_v$ ,  $c_v^e$ , and  $m_v$  are material parameters,  $H$  represents the hardening parameter,  $\eta = q/p$  represents the stress ratio, and  $M$  denotes the critical state stress ratio. The parameter  $m_v$  is an exponent controlling the isotropic compression behavior. It should be noted that in the deviatoric stress term of Eq. (2), the factor  $m_v/(2 - m_v)$  is introduced to ensure that when  $\eta = M$ ,  $\partial f/\partial p$  is identically zero. This guarantees that, regardless of the value of  $m_v$ , the critical state line passes  $q = Mp$  through the apex of all yield surfaces in the  $(p, q)$  plane. The value of  $m_v$  modifies the elliptical yield surface into a teardrop yield surface.

Fig. 1 illustrates the yield surface shapes for different  $m_v$  values when  $M$  is set to 1.5. It is evident that when  $m_v < 1$ ,

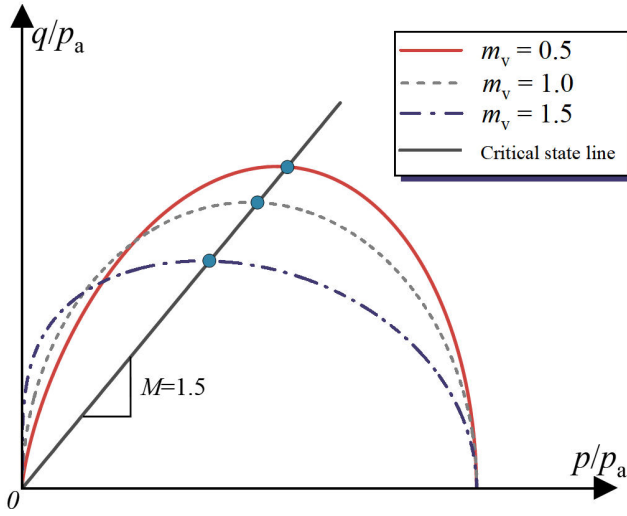


Fig. 1 The yield surface shapes with different  $m_v$ .

the yield surface tilts positively along the  $p$ -axis, and when  $m_v > 1$ , the yield surface tilts negatively along the  $p$ -axis. When  $m_v = 1$ , the yield surface takes the same elliptical shape as the modified Cambridge model (MCC Model).

### 2.3 Dilatancy equation

This study investigates the weakly weathered granite rockfill materials with the same gradation and preparation dry density ( $\rho_d = 2.07 \text{ g/cm}^3$ ) under four different confining pressures ( $\sigma_3 = 300, 600, 1000, 1500 \text{ kPa}$ ) through consolidation-drained shear (CD) tests. The particle distribution of the rockfill material, including both the designed and scaled (tested) materials, is shown in Fig. 2, and the test results are presented in Fig. 3. For the rockfill material, the initial deviatoric stress increases rapidly with axial strain. The initial tangential modulus shows a roughly positive correlation with the confining pressure. As shear progresses, the rearrangement and reorganization of the rockfill particles lead to a continuous reduction in the tangential modulus. Once the axial strain reaches a certain value, the deviatoric stress first reaches a peak and then exhibits a distinct strain-softening behavior. Furthermore, with increasing confining pressure, the peak deviatoric stress increases significantly, and the compressive strain becomes more pronounced. Throughout the entire testing process, shear dilation was observed at both low and high confining pressures, with the phenomenon being more pronounced at lower confining pressures.

Fig. 4 illustrates the effective stress paths and directions of plastic strain increments observed in the triaxial tests conducted on the weakly weathered granite rockfill

material in this study. A key aspect of Fig. 4 is the envelope of the peak-state stress ratio (solid blue line) and the critical dilatancy stress ratio (dashed blue line). It is observed that both stress ratios decrease with increasing confining pressure. Fu et al. [6] effectively characterized the aforementioned envelope using a power-function formulation, as given:

- Envelope of peak stress state is:

$$\frac{q}{p_a} = r_f \left( \frac{p}{p_a} \right)^{n_f} . \quad (4)$$

In Eq. (4),  $r_f$  and  $n_f$  are material parameters. For the CD tests shown in Fig. 3, these parameters are  $r_f = 2.66$  and  $n_f = 0.88$ . The expression of peak stress ratio  $M_f$  is as follows:

$$M_f = r_f \left( \frac{p}{p_a} \right)^{n_f - 1} . \quad (5)$$

- Envelope of critical dilatancy stress state is:

$$\frac{q}{p_a} = r_c \left( \frac{p}{p_a} \right)^{n_c} . \quad (6)$$

In Eq. (6),  $r_c$  and  $n_c$  are material parameters. For the CD tests shown in Fig. 3, these parameters are  $r_c = 2.25$  and  $n_c = 0.92$ . The expression of critical dilatancy stress ratio  $M_c$  is as follows:

$$M_c = r_c \left( \frac{p}{p_a} \right)^{n_c - 1} . \quad (7)$$

The first step in establishing the dilatancy relationship is to plot the relationship between the dilatancy ratio and the stress ratio using experimental data from the conventional triaxial tests shown in Fig. 3, as presented in Fig. 5 (a). It is observed that when the stress ratio is less than 1.0, significant data scatter occurs, particularly during the initial shear stages. This phenomenon can be attributed to several factors, such as the influence of the initial fabric [30] or the frictional constraints at the specimen ends [31, 32]. Additionally, some scattering is observed near the dilatancy zone. To account for particle breakage, Fu et al. [6] incorporated the critical dilatancy stress ratio  $M_c$  into the dilatancy equation and proposed the following nonlinear formulation:

$$d = d_0 \left[ 1 - \left( \frac{\eta}{M_c} \right)^{d_n} \right] . \quad (8)$$

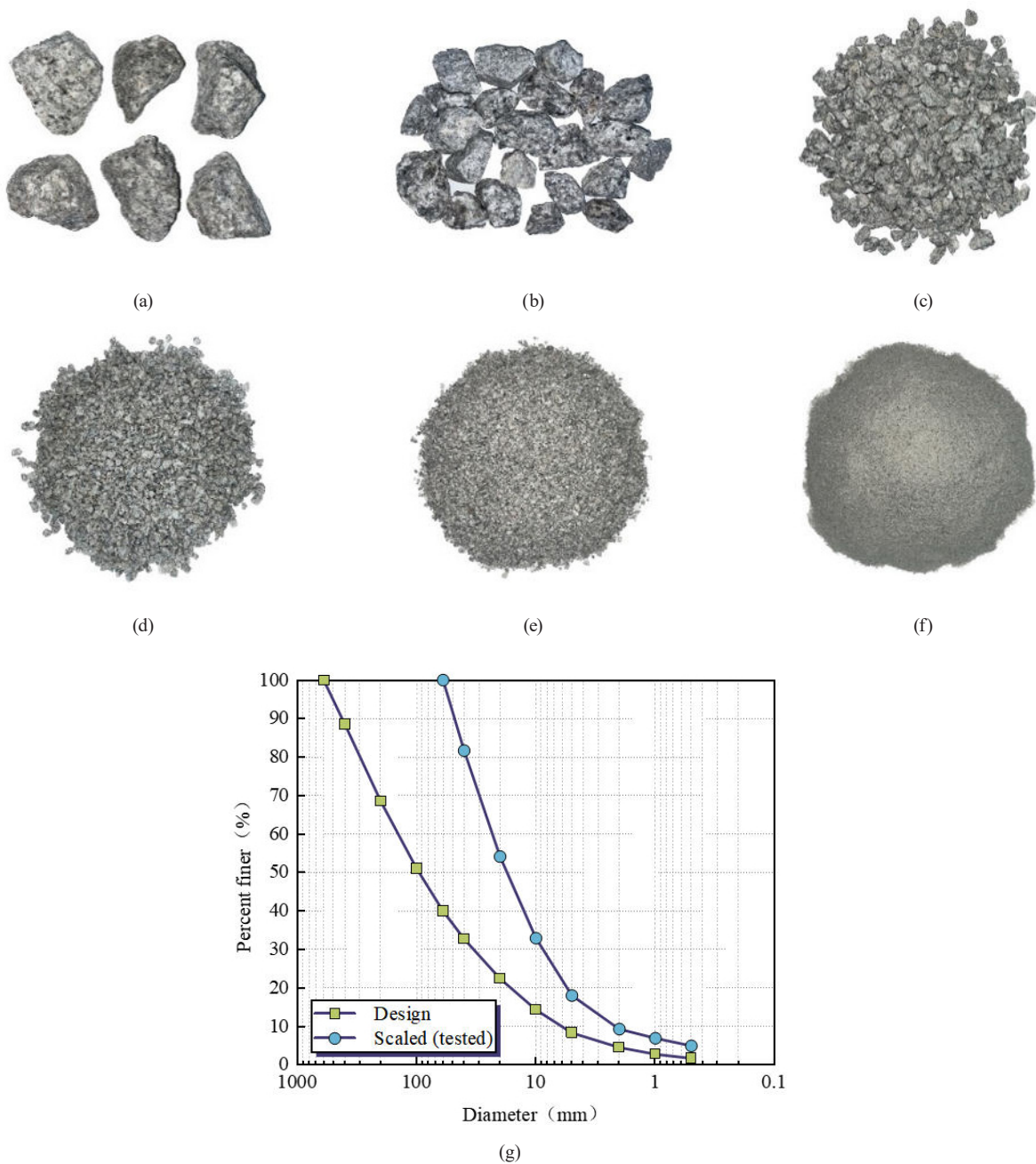


**Fig. 2** The particle distribution of the weakly weathered granite rockfill material: (a) Grain size groups: 60~40 mm, (b) Grain size groups: 40~20 mm, (c) Grain size groups: 20~10 mm, (d) Grain size groups: 10~5 mm, (e) Grain size groups: 5~2 mm, (f) Grain size groups: <2 mm, (g) Engineering grading curve and test grading curve

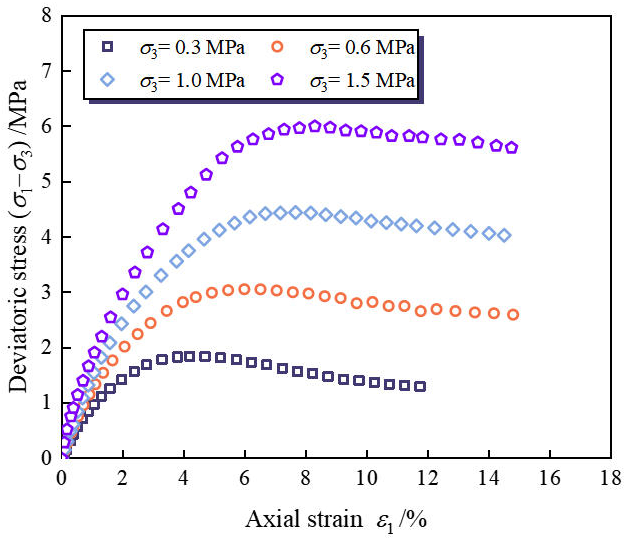
In Eq. (8),  $d_0$  represents the initial dilatancy ratio, which numerically corresponds to the vertical intercept when  $\eta = 0$ .  $M_c$  is the critical dilatancy stress ratio.

Based on conventional triaxial test data for weakly weathered granite rockfill, the relationship between dilatancy ratio and normalized stress ratio is provided (Fig. 5 (b)), with  $d_0 = 0.66$  and  $d_n = 3.5$ . It can be observed that the above dilatancy equation effectively models the

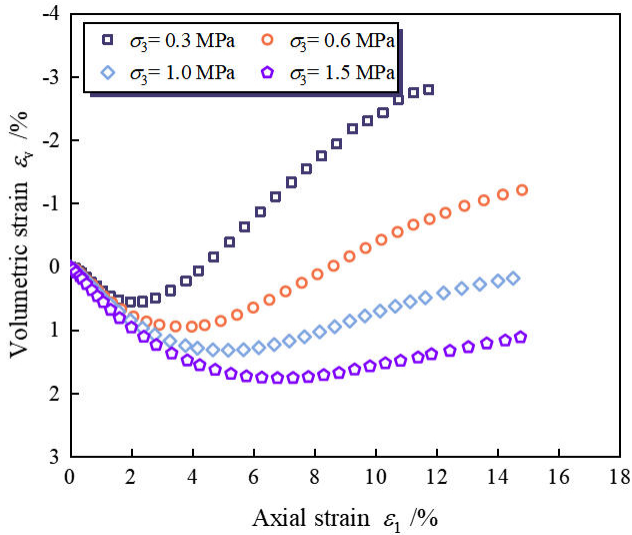
variation between the dilatancy ratio and normalized stress ratio under different confining pressures.

#### 2.4 Construction of stress-path-independent hardening parameters for rockfill materials

Research has shown that the plastic work  $W^P$  generated by loading along different stress paths from a given stress point to another yield surface is nearly independent of the



(a)



(b)

**Fig. 3** Results of conventional triaxial compression test of weakly weathered granite rockfill: (a) Deviatoric stress–Axial strain, (b) Volumetric strain–Axial strain

stress path [33]. Since plastic work reflects the dilatancy behavior of soils, it is considered a potential hardening parameter for rockfill materials. The expression for plastic work is as follows:

$$W^P = \int dW^P = \int p d\varepsilon_v^p + q d\varepsilon_s^p = \int p(d\varepsilon_v^p + \eta d\varepsilon_s^p). \quad (9)$$

The Contours of volumetric strain and plastic work in the  $p$ – $q$  space were plotted using the experimental data from Fig. 3, as shown in Fig. 6. It can be observed that the contours of plastic volumetric strain differ significantly from ellipses, particularly at lower levels of mean normal stress. In contrast, the contours of plastic work are closer

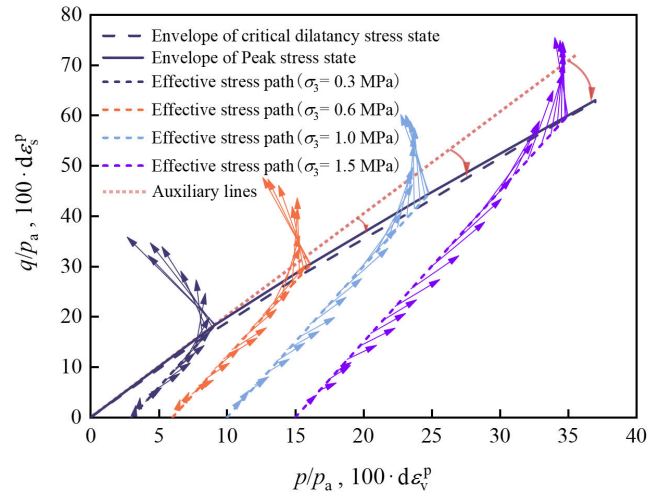
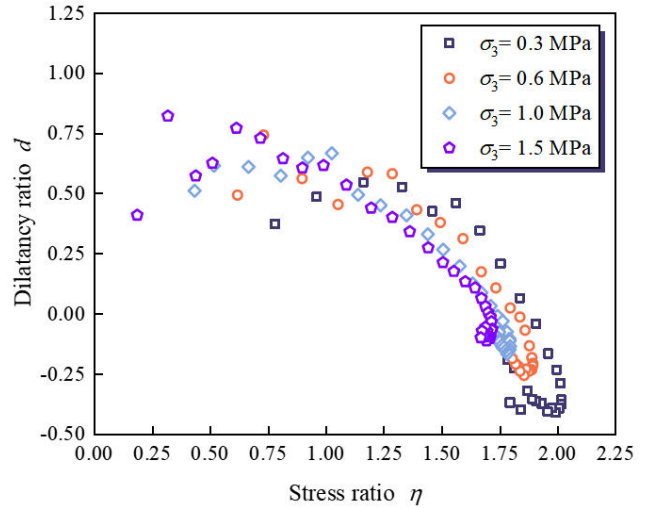
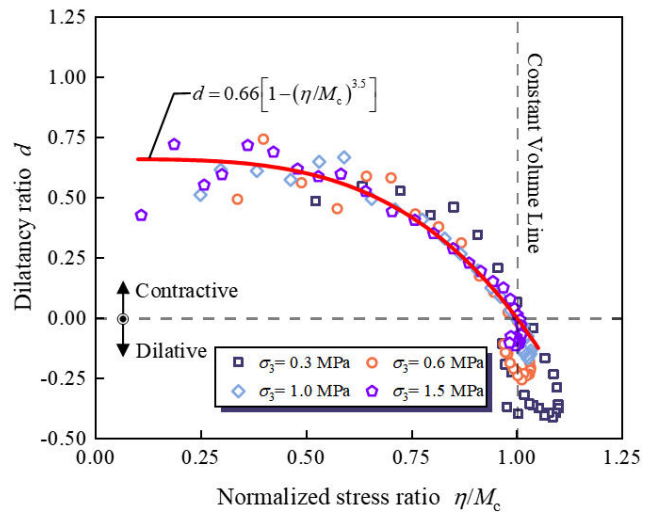


**Fig. 4** Effective stress paths and directions of plastic strain increments from the triaxial test



(a)



(b)

**Fig. 5** The relationship between the dilatation ratio and the stress ratio of the rockfill: (a)  $d$ – $\eta$ , (b)  $d$ – $\eta/M_c$

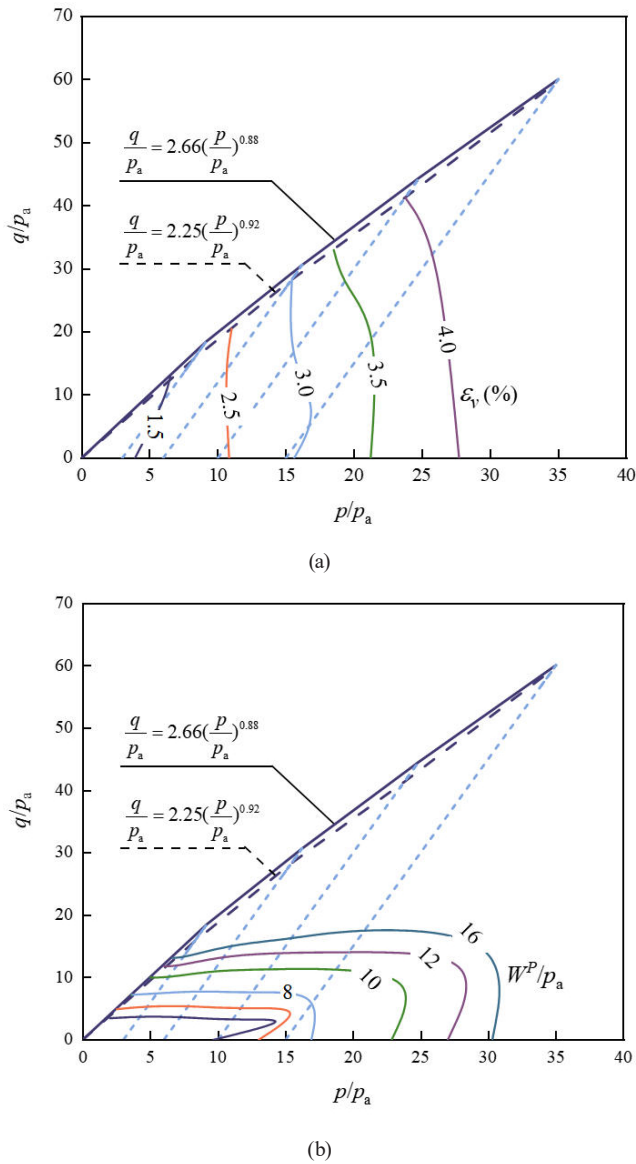


Fig. 6 The contours of (a) volumetric strain and (b) plastic work in the  $p$ - $q$  space

to ellipses. It should be noted that, due to the unknown nature of elastic behavior, the contours in this context were drawn using total volumetric strain. In practice, the contribution of elastic strain to plastic volumetric strain and plastic work is minimal, so the actual contours will not differ substantially from those shown in Fig. 6.

Although plastic work satisfies the basic conditions for being a hardening parameter, it is not an ideal choice. Studies have shown [15, 16] that stress paths with different mean normal stresses but the same stress ratio increment should exhibit similar shear characteristics, resulting in approximately equal increments of plastic volumetric strain and plastic shear strain, with corresponding increments of the hardening parameter also being similar.

However, the actual increments of plastic work can differ significantly. Section 2.5 provides a detailed method for constructing a stress-path-independent hardening parameter suitable for rockfill materials.

The construction method for the hardening parameter  $H$  is introduced based on the previously established yield function. Let  $c_p = c_v - c_v^e$ , then the yield function in Eq. (2) can be rewritten as

$$f(p, q, H) = \left(\frac{p}{p_a}\right)^{m_v} \left(1 + \frac{m_v}{2 - m_v} \frac{q^2}{M^2 p^2}\right) - \frac{1}{c_p} H = 0. \quad (10)$$

The hardening parameter  $H$  can be expanded as follows:

$$H = \int \frac{d\varepsilon_v^p}{R(\eta)}. \quad (11)$$

In Eq. (11),  $R(\eta)$  represents the stress-path-related factor, where  $R(\eta) = 1$  in the modified Cambridge model. From Eqs. (10) and (11), the total differential form of the yield function can be derived as

$$df = \frac{\partial f}{\partial p} dp + \frac{\partial f}{\partial q} dq - \frac{1}{c_p} \frac{d\varepsilon_v^p}{R(\eta)} = 0. \quad (12)$$

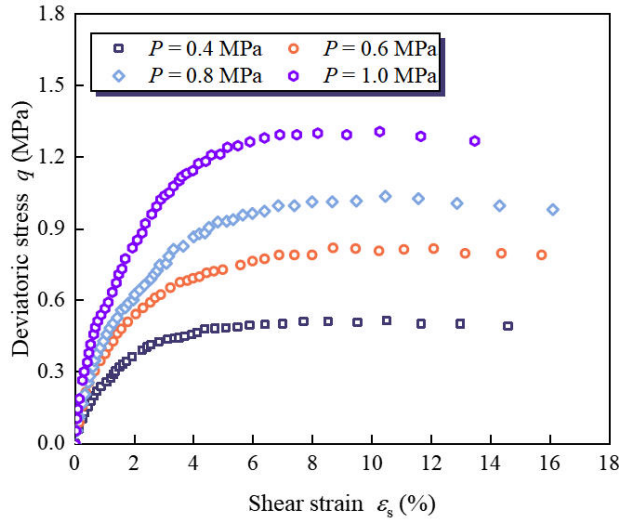
For normally consolidated clays or soils with minimal dilatancy, it can be assumed that the characteristic state transitioning from contractive to dilative behavior coincides with the critical state. Therefore, both the critical dilatancy stress ratio and the critical state stress ratio are represented by  $M$ . By introducing the dilatancy equation, Eq. (11) can be transformed into

$$\begin{cases} d\varepsilon_v^p = c_p R(\eta) \left( \frac{\partial f}{\partial p} dp + \frac{\partial f}{\partial q} dq \right) \\ d\varepsilon_s^p = c_p R(\eta) \frac{1}{d_0} \frac{M^{d_n}}{M^{d_n} - \eta^{d_n}} \left( \frac{\partial f}{\partial p} dp + \frac{\partial f}{\partial q} dq \right) \end{cases}. \quad (13)$$

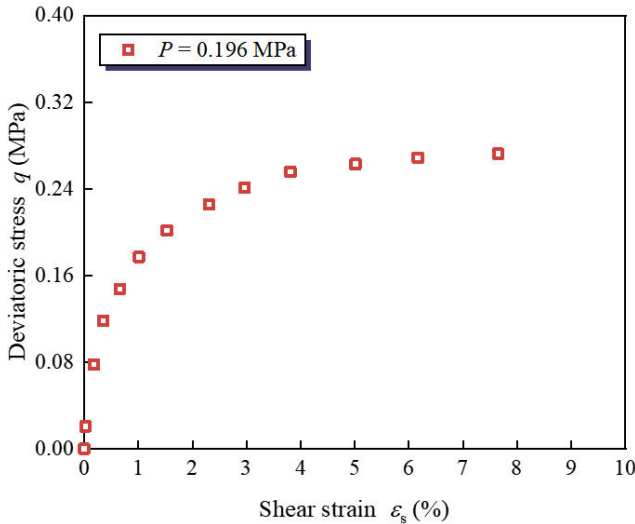
In the constant  $p$  stress path, it is known that  $dp = 0$ , and the plastic shear strain increment can be expressed as

$$dq = \frac{d_0}{c_p} \frac{2 - m_v}{m_v} \frac{p_a^{m_v}}{p^{m_v - 1}} \frac{1}{R(\eta)} \frac{M^{d_n} - \eta^{d_n}}{M^{d_n - 2}} \frac{1}{2\eta} d\varepsilon_s^p. \quad (14)$$

Based on the experimental results from references [14, 34], the  $q$ - $\varepsilon_s$  relationship curves for rockfill and clay along the constant  $p$  stress path are compiled, as shown in Fig. 7. It can be observed that the shear curves for rockfill and clay are similar, with the primary difference being the peak stress ratio. Normally consolidated clay exhibits monotonous volumetric compression along the constant  $p$  stress path, with both the critical dilatancy



(a)



(b)

 Fig. 7 The  $\varepsilon_s$ - $\eta$  curves of (a) rockfill and (b) clay

stress ratio and the critical state stress ratio equal to  $M$ . In contrast, rockfill may experience dilatancy before reaching the peak stress ratio, resulting in a peak stress ratio  $M_f$  that exceeds the dilatancy stress ratio  $M$ .

For normally consolidated soils, with  $R(\eta) = 1$  in the modified Cambridge model, the relationship between the deviatoric stress increment and the incremental plastic shear strain in Eq. (14) is given by

$$dq = \frac{d_0}{c_p} \frac{2-m_v}{m_v} \frac{p_a^{m_v}}{p^{m_v-1}} \frac{M^{d_n} - \eta^{d_n}}{M^{d_n-2}} \frac{1}{2\eta} d\varepsilon_s^p. \quad (15)$$

Considering that the  $\varepsilon_s$ - $\eta$  curves of rockfill and clay are similar under the constant  $p$  stress path, the relationship between the deviatoric stress increment and the plastic shear strain increment of the rockfill is assumed to be:

$$dq = \rho \frac{d_0}{c_p} \frac{2-m_v}{m_v} \frac{p_a^{m_v}}{p^{m_v-1}} \frac{M^{d_n} - \eta^{d_n}}{M^{d_n-2}} \frac{1}{2\eta} d\varepsilon_s^p. \quad (16)$$

In Eq. (16),  $\rho$  is an undetermined coefficient, representing the ratio of incremental plastic shear strain between rockfill and clay. Equations (15) and (16) can be respectively transformed into the relationship between shear modulus and stress state, as follows:

- Clay

$$G_t = \frac{3d_0}{c_p} \frac{2-m_v}{m_v} \frac{p_a^{m_v}}{p^{m_v-1}} \frac{M^{d_n} - \eta^{d_n}}{M^{d_n-2}} \frac{1}{2\eta} \quad (17)$$

- Rockfill

$$G_t = \rho \frac{3d_0}{c_p} \frac{2-m_v}{m_v} \frac{p_a^{m_v}}{p^{m_v-1}} \frac{M_f^{d_n} - \eta^{d_n}}{M_f^{d_n-2}} \frac{1}{2\eta}. \quad (18)$$

It should be noted that the variables on the right-hand side of Eqs. (17) and (18) are structurally similar. These variables can be transformed into:

- Clay

$$\frac{M^{d_n} - \eta^{d_n}}{M^{d_n-2}} \frac{1}{2\eta} = \frac{M}{2} \left[ \frac{M}{\eta} - \left( \frac{\eta}{M} \right)^{d_n-1} \right] \quad (19)$$

- Rockfill

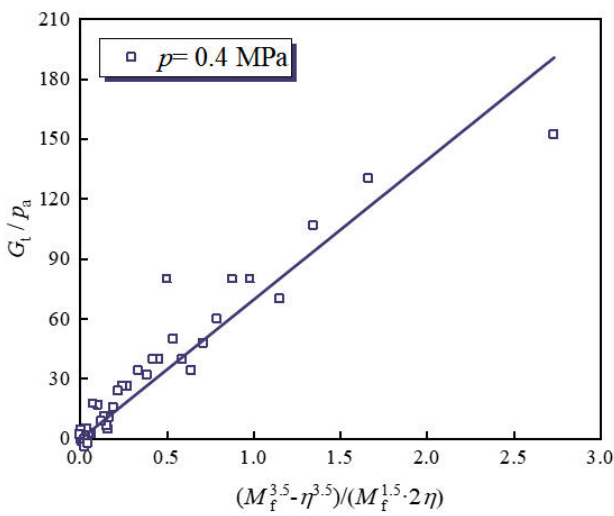
$$\frac{M_f^{d_n} - \eta^{d_n}}{M_f^{d_n-2}} \frac{1}{2\eta} = \frac{M_f}{2} \left[ \frac{M_f}{\eta} - \left( \frac{\eta}{M_f} \right)^{d_n-1} \right]. \quad (20)$$

For the rockfill material used in this study, the dilatancy parameter is  $d_n = 3.5$ . Based on experimental results from references [14, 34], the relationships between  $G_t - (M_f^{3.5} - \eta^{3.5}) / (M_f^{1.5} \cdot 2\eta)$  and  $G_t - (M^{3.5} - \eta^{3.5}) / (M^{1.5} \cdot 2\eta)$  were derived, as shown in Figs. 8 and 9. It can be observed that, after processing the coordinate system, both the rockfill material and clay approximate straight lines passing through the origin, with only differences in slope magnitude.

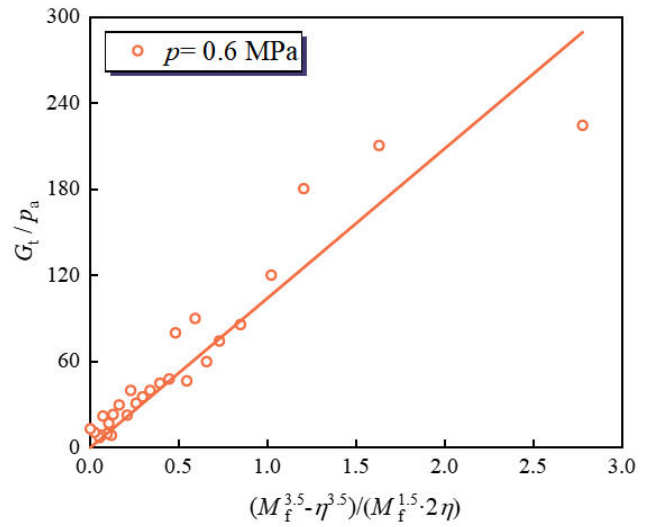
By simultaneously solving Eqs. (11), (14), and (18), and incorporating the plastic volumetric strain variation under the isotropic compression stress path as described in Eq. (10), the hardening parameter can be determined as

$$H = \int \frac{1}{R(\eta)} d\varepsilon_v^p = \int \frac{M^{d_n} (M_f^{d_n} - \eta^{d_n})}{M_f^{d_n} (M^{d_n} - \eta^{d_n})} d\varepsilon_v^p. \quad (21)$$

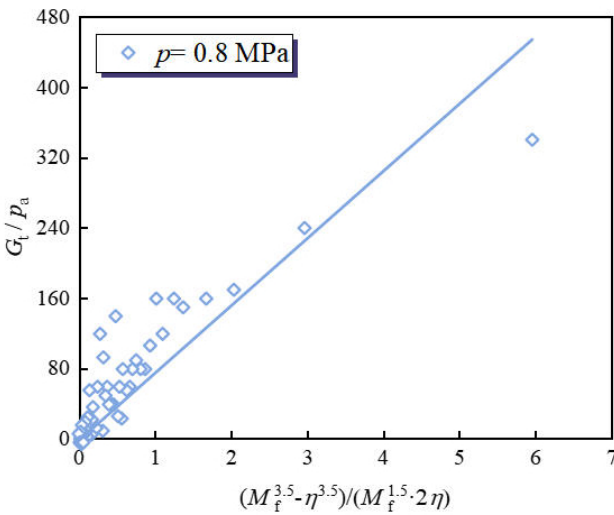
It can be observed that in Eq. (21), the hardening parameter  $H$ , which is independent of the stress path, is composed of



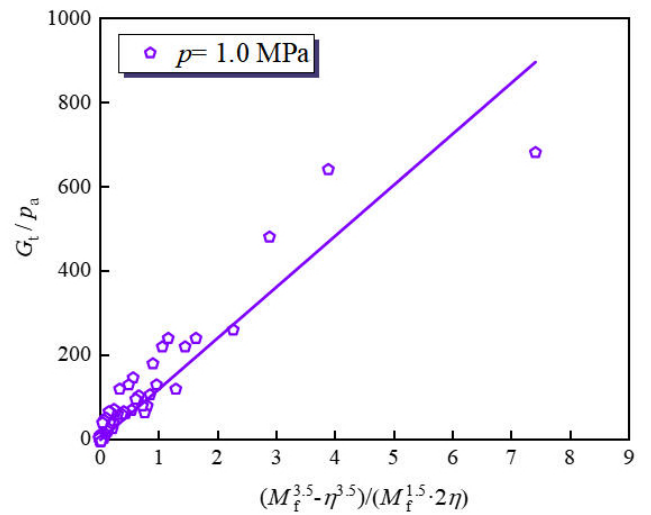
(a)



(b)



(c)



(d)

**Fig. 8** The  $G_t - (M_f^{3.5} - \eta^{3.5}) / (M_f^{1.5} \cdot 2\eta)$  curve of rockfill: (a) rockfill ( $p = 0.4$  MPa), (b) rockfill ( $p = 0.6$  MPa), (c) rockfill ( $p = 0.8$  MPa), (d) rockfill ( $p = 1.0$  MPa)

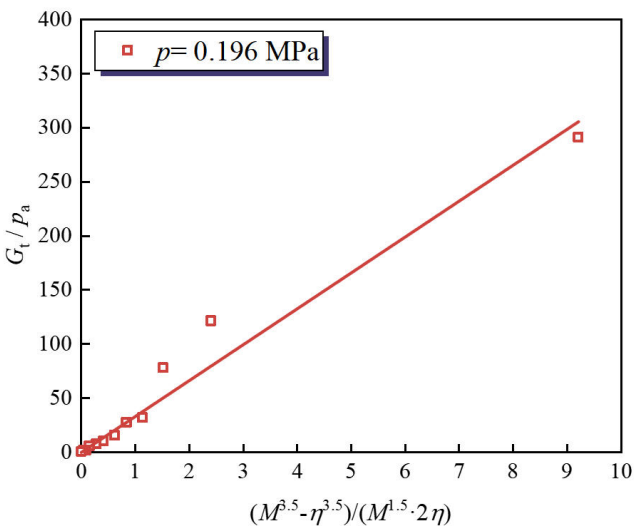


**Fig. 9** The  $G_t - (M_f^{3.5} - \eta^{3.5}) / (M_f^{1.5} \cdot 2\eta)$  curve of clay

two stress-path-dependent parameters: the plastic volumetric strain increment  $\varepsilon_v^p$  and the stress path-related factor  $R(\eta)$ .

Based on the test results shown in Fig. 3, iso-contours of the hardening parameter  $H$  in the  $p$ - $q$  space were plotted, as shown in Fig. 10. It can be observed that across a wide range of mean effective stress, the contours of  $H$  resemble elliptical surfaces. Notably, the right-leaning, droplet-shaped yield surface (with  $m_v = 0.5$ ) shown in Fig. 1 aligns well with the contour pattern of the hardening parameter  $H$ .

By substituting the expression for the hardening parameter  $H$  into Eq. (10), the yield function takes the following form:

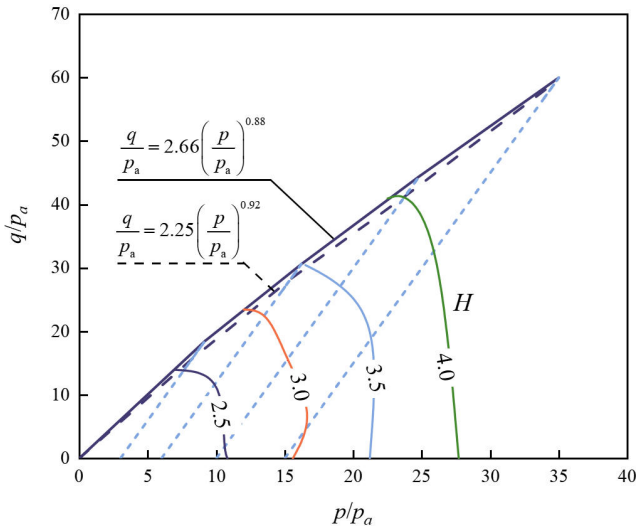


Fig. 10 Contours of hardening parameter  $H$  on  $p$ - $q$  plane

$$f(p, q, H) = c_p \left( \frac{p}{p_a} \right)^{m_v} \left( 1 + \frac{m_v}{2 - m_v} \frac{q^2}{M^2 p^2} \right) - \int \frac{M^{d_n} (M_f^{d_n} - \eta^{d_n})}{M_f^{d_n} (M^{d_n} - \eta^{d_n})} d\varepsilon_v^p = 0 \quad (22)$$

### 2.5 Stress-strain relationship of elastoplastic constitutive model

By transforming the plastic strain increment formulation in Eq. (13), the matrix form of the plastic compliance is derived.

$$[C^p] = c_p R(\eta) \frac{1}{p} \left( \frac{p}{p_a} \right)^{m_v} \frac{m_v}{2 - m_v} \begin{bmatrix} \frac{(M^2 - \eta^2)(2 - m_v)}{M^2} & \frac{2\eta}{M^2} \\ \frac{(M^2 - \eta^2)(2 - m_v)}{d_0} \frac{M^{d_n-2}}{M^{d_n} - \eta^{d_n}} & \frac{2\eta}{d_0} \frac{M^{d_n-2}}{M^{d_n} - \eta^{d_n}} \end{bmatrix} \quad (23)$$

### 3 Constitutive model parameters

The proposed elastoplastic constitutive model for rockfill materials under stress loading consists of four parameter groups:

1. Bulk modulus parameters:  $k_v, k_v^e, m$ ;
2. Shear modulus parameters:  $k_s, k_s^e, n$ ;
3. Characteristic stress state parameters:  $r_c, n_c, r_f, n_f$ ;
4. Loading-induced dilatancy parameters:  $d_0, d_n$ .

Table 1 summarizes these parameters based on the corresponding experimental tests. The model requires a total of 12 parameters, all of which can be determined from two standard laboratory geotechnical tests.

Table 1 Constitutive model parameters and calibration

Type of parameter	Parameters	Types of tests
Bulk modulus parameters	$k_v, k_v^e, m$	Isotropic compression test
Shear modulus parameters	$k_s, k_s^e, n$	Conventional triaxial compression test
Characteristic stress state parameters	$r_c, n_c, r_f, n_f$	
Loading-induced dilatancy parameters	$d_0, d_n$	

### 3.1 Calibration of bulk modulus parameters

The methods for determining the characteristic stress state parameter, the dilatancy parameter, and the material parameters can be found in Sections 2.1 and 2.3. Below, the calibration methods for the bulk modulus and shear modulus parameters are provided separately.

The relationship between the plastic strain increment and the stress increment can be expressed as follows:

$$\begin{Bmatrix} d\varepsilon_v^p \\ d\varepsilon_s^p \end{Bmatrix} = [C^p] \begin{Bmatrix} dp \\ dq \end{Bmatrix} = \begin{bmatrix} C_{pp}^p & C_{pq}^p \\ C_{qp}^p & C_{qq}^p \end{bmatrix} \begin{Bmatrix} dp \\ dq \end{Bmatrix} = \begin{bmatrix} \frac{1}{K_{vv}^p} & \frac{1}{K_{vs}^p} \\ \frac{1}{K_{sv}^p} & \frac{1}{K_{ss}^p} \end{bmatrix} \begin{Bmatrix} dp \\ dq \end{Bmatrix} \quad (24)$$

Under the isotropic compression stress path, both the deviatoric stress and deviatoric strain vanish. Consequently, the Eq. (24) simplifies into independent equations:

$$d\varepsilon_v^p = \frac{1}{K_{vv}^p} dp. \quad (25)$$

By incorporating the elastic volumetric strain increment, the Eq. (26) is obtained:

$$d\varepsilon_v = d\varepsilon_v^e + d\varepsilon_v^p = \frac{1}{K} dp = \left( \frac{1}{K^e} + \frac{1}{K_{vv}^p} \right) dp. \quad (26)$$

Based on the distribution of volumetric strain under different confining pressures in isotropic compression tests, the experimental data can be fitted using a power function, as illustrated in Fig. 11. The fitted power function is expressed as follows:

$$\varepsilon_v = c_v \left( \frac{p}{p_a} \right)^{m_v}. \quad (27)$$

In Eq. (27),  $c_v = 25$  and  $m_v = 0.51$ . By differentiating the Eq. (27), the bulk modulus  $K$  can be obtained as follows:

$$K = \frac{dp}{d\varepsilon_v} = k_v p_a \left( \frac{p}{p_a} \right)^m. \quad (28)$$

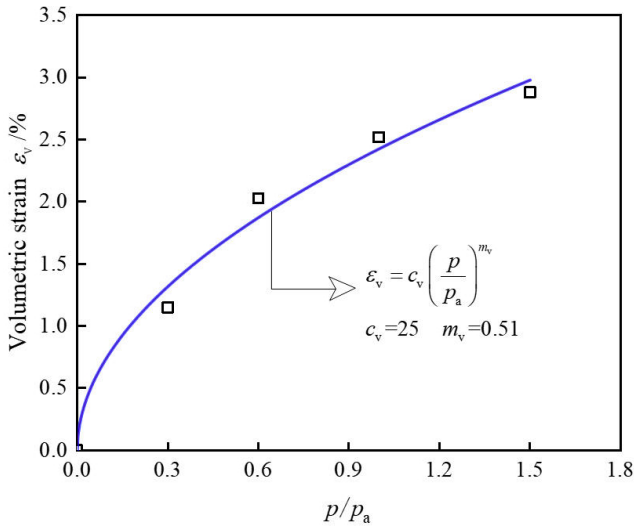


Fig. 11 The relationship between volume strain and mean normal stress in isotropic compression test

In Eq. (28),  $k_v = 1/(m_v c_v)$  and  $m = 1 - m_v$ . For saturated granite rockfill, the parameters are  $k_v = 7.9$  and  $m = 0.49$ . It should be noted that, to prevent excessive model parameters, the elastic bulk modulus in Eq. (1) also adopts the same power exponent  $m$ .

### 3.2 Calibration of shear modulus parameters

The initial tangent modulus  $G_0$  is determined based on triaxial compression test results under different confining pressures. Previous studies [35] have shown that in triaxial compression tests, the stress-strain relationship of materials often deviates from the hyperbolic assumption at both low and high stress levels, introducing significant uncertainty in the determination of model parameters. Consequently, substantial errors may arise in the estimation of  $G_0$ . In this study, the polynomial fitting method for stress-strain data is employed to determine  $G_0$  for each confining pressure condition in the experiments. Furthermore, its relationship with the mean normal stress is established. As illustrated in Fig. 12, this relationship can be expressed using the following power function:

$$G_0 = k_s p_a \left( \frac{p}{p_a} \right)^n \quad (29)$$

In Eq. (29),  $k_s$  and  $n$  are model parameters. For the saturated granite rockfill material in this study,  $k_s = 288.4$  and  $n = 0.33$ . Similarly, to reduce the number of model parameters, the same power exponent  $n$  is used in both Eq. (29) and Eq. (1).

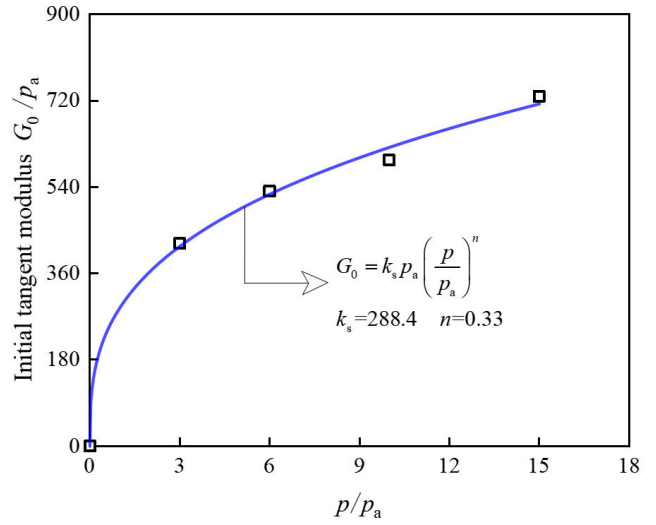


Fig. 12 The relationship between the initial tangent modulus and the mean normal stress

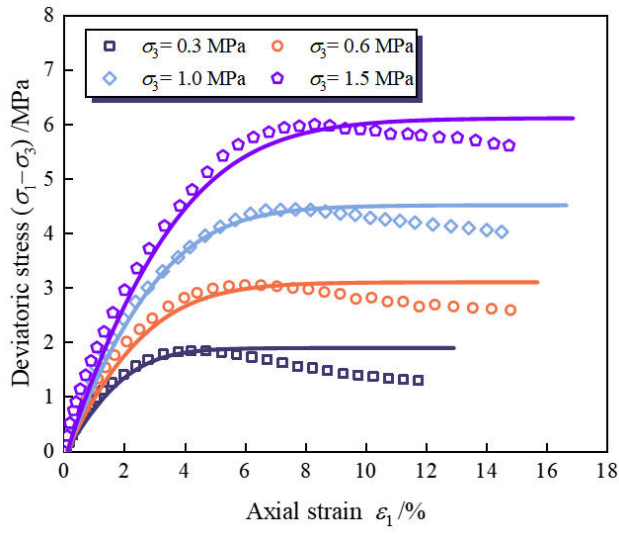
## 4 Model verification

First, the proposed model was validated using triaxial compression tests on granite rockfill material. Table 2 presents the elastoplastic constitutive model parameters determined from the experimental results, while Fig. 13 illustrates the simulation outcomes. The experimental data are represented as scattered points, whereas the simulated stress-strain responses are shown as curves. The results indicate that the model accurately captures both axial and volumetric strain behaviors, closely matching the experimental data. Additionally, the model effectively replicates the dilatancy behavior of rockfill material during shear. It is noted that, due to the influence of the nonlinear dilatancy equation fitting, the model tends to underestimate the rate of dilatancy evolution under low confining pressures. However, this limitation does not significantly impact the overall accuracy of the simulation.

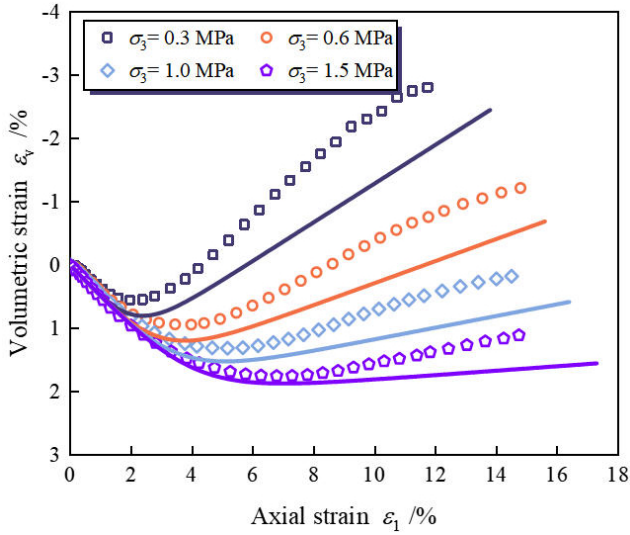
Furthermore, the model was validated using triaxial compression tests on two different types of dam construction rockfill materials [6, 36]. The elastoplastic constitutive model parameters for these materials are summarized in Tables 3 and 4, while Figs. 14 and 15 present the corresponding simulation results. A comparison between

Table 2 The fitting parameters of elastoplastic constitutive model of weakly weathered granite

$k_v$	$k_v^e$	$m$	$k_s$	$k_s^e$	$n$
7.9	39.5	0.49	288.4	1442.0	0.33
$r_c$	$n_c$	$r_f$	$n_f$	$d_0$	$d_n$
2.191	0.928	2.659	0.877	0.66	3.5



(a)



(b)

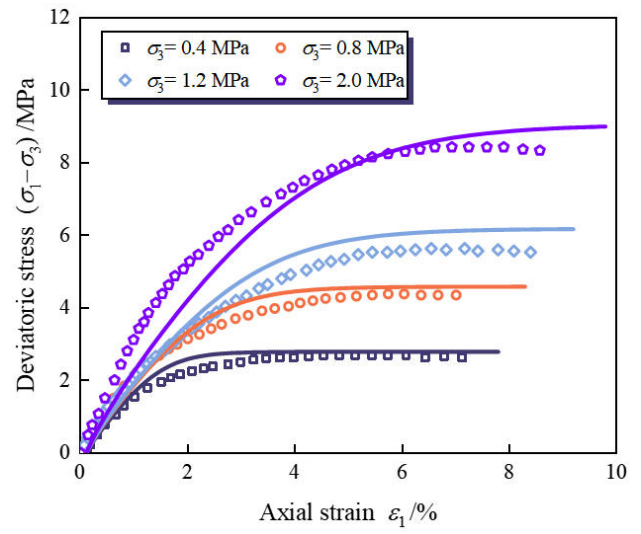
**Fig. 13** Fitting results of triaxial compression experiments on granite with the proposed model: (a) Deviatoric stress–Axial strain, (b) Volumetric strain–Axial strain

**Table 3** The fitting parameters of a rockfill [6] elastoplastic constitutive model

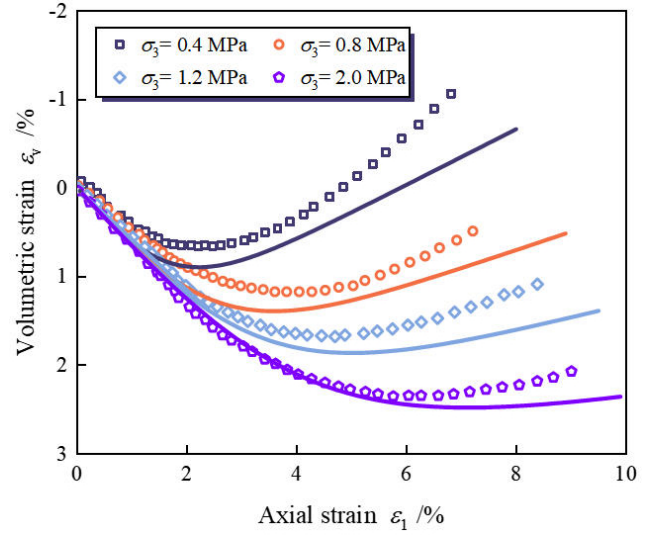
$k_v$	$k_v^e$	$m$	$k_s$	$k_s^e$	$n$
4.01	20.05	0.32	450.5	2252.5	0.34
$r_c$	$n_c$	$r_f$	$n_f$	$d_0$	$d_n$
2.31	0.92	2.77	0.88	0.75	4.0

**Table 4** The fitting parameters of a rockfill [36] elastoplastic constitutive model

$k_v$	$k_v^e$	$m$	$k_s$	$k_s^e$	$n$	$K_0$
2.51	12.55	0.31	147.8	739.0	0.46	0.245
$r_c$	$n_c$	$r_f$	$n_f$	$d_0$	$d_n$	$\alpha$
2.18	0.92	2.18	0.92	0.85	4.0	0.8



(a)



(b)

**Fig. 14** Fitting results of triaxial compression experiments on the rockfill material with the proposed model: (a) Deviatoric stress–Axial strain, (b) Volumetric strain–Axial strain

the experimental and simulated results demonstrates that the model effectively reproduces the triaxial compression responses under various confining pressures. It successfully captures key characteristics, including the nonlinear stress-strain relationship, dilatancy, and contraction behavior, for both types of rockfill materials.

### 5 Conclusions

Based on triaxial compression test data of weakly weathered granite rockfill material, an elastoplastic constitutive model for stress loading in rockfill was developed. The key features of the proposed model and the main findings are summarized as follows:

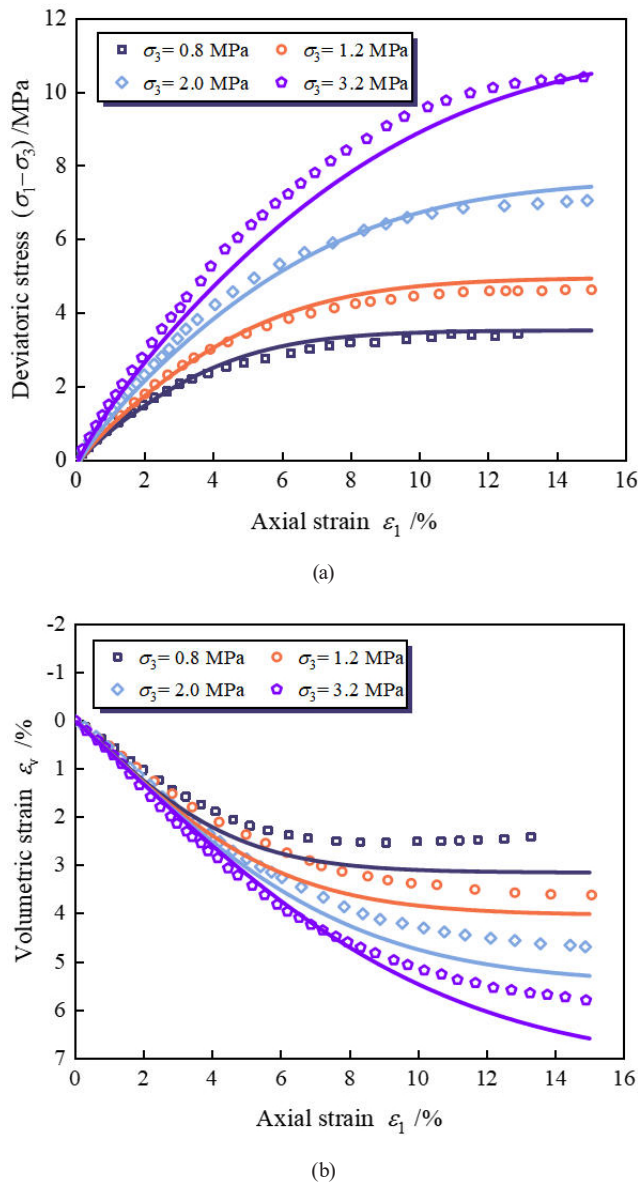


**Fig. 15** Fitting results of triaxial compression experiments on the rockfill material with the proposed model: (a) Deviatoric stress–Axial strain, (b) Volumetric strain–Axial strain

1. A teardrop yield function capable of controlling leftward and rightward tilting of the yield surface was constructed by introducing a factor with an isotropic

## References

[1] Lehner, B., Liermann, C. R., Revenga, C., Vörösmarty, C., Fekete, B., ..., Wissler, D. "Global Reservoir and Dam (GRanD) database", University of Washington, Seattle, WA, USA, Technical Documentation, Version 1.1, 2011.

[2] Rasskazov, L. N., Yadgorov, E. K., Burenkov, P. M. "Pore pressure dissipation in the core of the Nurek dam", *Power Technology and Engineering*, 50(1), pp. 54–59, 2016.  
<https://doi.org/10.1007/s10749-016-0658-y>

compression power exponent into the deviatoric stress term. This function can be regarded as an extension of the MCC model.

2. To account for particle breakage in rockfill materials, the critical dilatancy stress ratio was incorporated into the dilatancy equation. A nonlinear expression for the dilatancy equation was fitted based on experimental data from weakly weathered granite.
3. A stress-path-independent hardening parameter was formulated by integrating the yield function with the nonlinear dilatancy equation. This formulation was derived based on the constant  $p$  stress path and isotropic compression stress path, ensuring its suitability for rockfill materials.
4. The proposed constitutive model consists of 12 parameters, all of which can be determined from two conventional laboratory geotechnical tests. The model's validity was further verified using experimental data from multiple rockfill materials.

The limitations of the proposed model must also be recognized. The model posits a power function relationship between the peak stress ratio and confining pressure, indicating that the peak stress ratio is invariant over the loading process. Thus, a key limitation is its inability to account for the strain-softening behavior seen by dense rockfill in triaxial compression experiments, when deviatoric stress and volumetric change typically settle. Formulating an evolution formula for the peak stress ratio or integrating the critical state idea may address this limitation.

## Acknowledgement

This study was supported by the Jiangsu Province Water Conservancy Science and Technology Project (No. 2024001), National Natural Science Foundation of China Excellent Young Scientist Fund: Earth-Rock Dam Engineering (52222906) and the National Natural Science Foundation of China (No. U21A20158, U2443232).

[3] Ma, H., Chi, F. "Major technologies for safe construction of high earth-rockfill dams", *Engineering*, 2(4), pp. 498–509, 2016.  
<https://doi.org/10.1016/J.ENG.2016.04.001>

[4] Chen, S.-S. "土石坝试验新技术研究与应用" (Experimental techniques for earth and rockfill dams and their applications), *Chinese Journal of Geotechnical Engineering*, 37(1), pp. 1–28, 2015. (in Chinese)  
<https://doi.org/10.11779/CJGE201501001>

- [5] Fu, Z., Chen, S., Shi, B. "Large-Scale Triaxial Experiments on the Creep Behavior of a Saturated Rockfill Material", *Journal of Geotechnical and Geoenvironmental Engineering*, 144(7), 04018039, 2018.  
[https://doi.org/10.1061/\(ASCE\)GT.1943-5606.0001898](https://doi.org/10.1061/(ASCE)GT.1943-5606.0001898)
- [6] Fu, Z., Chen, S., Zhong, Q., Zhang, Y. "Modeling interaction between loading-induced and creep strains of rockfill materials using a hardening elastoplastic constitutive model", *Canadian Geotechnical Journal*, 56(10), pp. 1380–1394, 2019.  
<https://doi.org/10.1139/cgj-2018-0435>
- [7] Alonso, E. E., Olivella, S., Pinyol, N. M. "A review of Beliche Dam", *Géotechnique*, 55(4), pp. 267–285, 2005.  
<https://doi.org/10.1680/geot.2005.55.4.267>
- [8] Elia, G., Amorosi, A., Chan, A. H. C., Kavvas, M. J. "Fully coupled dynamic analysis of an earth dam", *Géotechnique*, 61(7), pp. 549–563, 2011.  
<https://doi.org/10.1680/geot.8.P.028>
- [9] Chen, S.-S., Fu, Z.-Z., Shi, B.-X., Yuan, J. "统一考虑加载变形与流变的粗粒土弹塑性本构模型及应用" (Elastoplasticity constitutive model considering loading-induced deformation and creep behavior of coarse granular soils and its application), *Chinese Journal of Geotechnical Engineering*, 41(4), pp. 601–609, 2019. (in Chinese)  
<https://doi.org/10.11779/CJGE201904001>
- [10] Liu, S.-H., Sun, Y., Shen, C.-M., Yin, Z.-Y. "Practical nonlinear constitutive model for rockfill materials with application to rockfill dam", *Computers and Geotechnics*, 119, 103383, 2020.  
<https://doi.org/10.1016/j.compgeo.2019.103383>
- [11] Chen, S.-S., Yan, Z.-K., Fu, Z.-Z., Li, G.-Y. "特高面板砂砾石坝结构安全性论证" (Evaluation of the safety performance of extremely high slab-faced gravel dam), *Chinese Journal of Geotechnical Engineering*, 39(11), pp. 1949–1958, 2017. (in Chinese)  
<https://doi.org/10.11779/CJGE201711001>
- [12] Kavvas, M., Amorosi, A. "A constitutive model for structured soils", *Géotechnique*, 50(3), pp. 263–273, 2000.  
<https://doi.org/10.1680/geot.2000.50.3.263>
- [13] Ti, K. S., Huat, B. B. K., Noorzaei, J., Jaafar, M. S., Sew, G. S. "A review of basic soil constitutive models for geotechnical application", *Electronic Journal of Geotechnical Engineering*, 14, pp. 1–18, 2009.
- [14] Nakai, T., Matsuoka, H. "A generalized elastoplastic constitutive model for clay in three-dimensional stresses", *Soils and Foundations*, 26(3), pp. 81–98, 1986.  
[https://doi.org/10.3208/sandf1972.26.3\\_81](https://doi.org/10.3208/sandf1972.26.3_81)
- [15] Lade, P. V., Kim, M. K. "Single hardening constitutive model for soil, rock and concrete", *International Journal of Solids and Structures*, 32(14), pp. 1963–1978, 1995.  
[https://doi.org/10.1016/0020-7683\(94\)00247-T](https://doi.org/10.1016/0020-7683(94)00247-T)
- [16] Yao, Y. P., Sun, D. A., Matsuoka, H. "A unified constitutive model for both clay and sand with hardening parameter independent on stress path", *Computers and Geotechnics*, 35(2), pp. 210–222, 2008.  
<https://doi.org/10.1016/j.compgeo.2007.04.003>
- [17] Schanz, T., Vermeer, P. A., Bonnier, P. G. "The hardening soil model: Formulation and verification", In: *Beyond 2000 in Computational Geotechnics*, Routledge, 1999, pp. 281–296. ISBN 9789058090409  
<https://doi.org/10.1201/9781315138206-27>
- [18] Roscoe, K. H., Schofield, A. N., Wroth, C. P. "On the yielding of soils", *Géotechnique*, 8(1), pp. 22–53, 1958.  
<https://doi.org/10.1680/geot.1958.8.1.22>
- [19] Hsieh, H. S., Kavazanjian, E., Borja, R. I. "Double-yield-surface cam-clay plasticity model. I: theory", *Journal of Geotechnical Engineering*, 116(9), pp. 1381–1401, 1990.  
[https://doi.org/10.1061/\(ASCE\)0733-9410\(1990\)116:9\(1381\)](https://doi.org/10.1061/(ASCE)0733-9410(1990)116:9(1381))
- [20] Varadarajan, A., Sharma, K. G., Venkatachalam, K., Gupta, A. K. "Testing and modeling two rockfill materials", *Journal of Geotechnical and Geoenvironmental Engineering*, 129(3), pp. 206–218, 2003.  
[https://doi.org/10.1061/\(ASCE\)1090-0241\(2003\)129:3\(206\)](https://doi.org/10.1061/(ASCE)1090-0241(2003)129:3(206))
- [21] Alonso, E. E., Romero, E. E., Ortega, E. "Yielding of rockfill in relative humidity-controlled triaxial experiments", *Acta Geotechnica*, 11(3), pp. 455–477, 2016.  
<https://doi.org/10.1007/s11440-016-0437-9>
- [22] Dolzyk-Szypcio, K. "Stress-Dilatancy of Rounded and Angular Rockfill Materials", *IOP Conference Series: Earth and Environmental Science*, IOP Publishing, 221(1), 012013, 2019.  
<https://doi.org/10.1088/1755-1315/221/1/012013>
- [23] Dafalias, Y. F. "Bounding surface plasticity. I: Mathematical foundation and hypoplasticity", *Journal of Engineering Mechanics*, 112(9), pp. 966–987, 1986.  
[https://doi.org/10.1061/\(ASCE\)0733-9399\(1986\)112:9\(966\)](https://doi.org/10.1061/(ASCE)0733-9399(1986)112:9(966))
- [24] Hashiguchi, K. "Subloading surface model in unconventional plasticity", *International Journal of Solids and Structures*, 25(8), pp. 917–945, 1989.  
[https://doi.org/10.1016/0020-7683\(89\)90038-3](https://doi.org/10.1016/0020-7683(89)90038-3)
- [25] Whittle, A. J., Kavvas, M. J. "Formulation of MIT-E3 constitutive model for overconsolidated clays", *Journal of Geotechnical Engineering*, 120(1), pp. 173–198, 1994.  
[https://doi.org/10.1061/\(ASCE\)0733-9410\(1994\)120:1\(173\)](https://doi.org/10.1061/(ASCE)0733-9410(1994)120:1(173))
- [26] Yao, Y.-P., Hou, W., Zhou, A.-N. "UH model: three-dimensional unified hardening model for overconsolidated clays", *Géotechnique*, 59(5), pp. 451–469, 2009.  
<https://doi.org/10.1680/geot.2007.00029>
- [27] Yao, Y. P., Niu, L., Cui, W. J. "Unified hardening (UH) model for overconsolidated unsaturated soils", *Canadian Geotechnical Journal*, 51(7), pp. 810–821, 2014.  
<https://doi.org/10.1139/cgj-2013-0183>
- [28] Guo, W.-L., Zhu, J.-G., Peng, W.-M. "粗粒土的剪胀方程及广义塑性本构模型研究" (Dilatancy equation and generalized plastic constitutive model for coarse-grained soils), *Chinese Journal of Geotechnical Engineering*, 40(6), pp. 1103–1110, 2018. (in Chinese)  
<https://doi.org/10.11779/CJGE201806016>
- [29] Fu, Z.-Z., Chen, S.-S., Zhang, Y.-J., Shi, B.-X. "堆石料加载与流变过程中塑性应变方向研究" (Plastic strain directions of rockfill materials during loading and creeping), *Chinese Journal of Geotechnical Engineering*, 40(8), pp. 1405–1414, 2018. (in Chinese)  
<https://doi.org/10.11779/CJGE201808005>
- [30] Been, K., Jefferies, M. "Stress-dilatancy in very loose sand", *Canadian Geotechnical Journal*, 41(5), pp. 972–989, 2004.  
<https://doi.org/10.1139/t04-038>
- [31] Jardine, R. J., Symes, M. J., Burland, J. B. "The measurement of soil stiffness in the triaxial apparatus", *Géotechnique*, 34(3), pp. 323–340, 1984.  
<https://doi.org/10.1680/geot.1984.34.3.323>

- [32] Clayton, C. R. I. "Stiffness at small strain: research and practice", *Géotechnique*, 61(1), pp. 5–37, 2011.  
<https://doi.org/10.1680/geot.2011.61.1.5>
- [33] Nakai T. "An isotropic hardening elastoplastic model for sand considering the stress path dependency in three-dimensional stresses", *Soils and Foundations*, 29(1), pp. 119–137, 1989.  
<https://doi.org/10.3208/sandf1972.29.119>
- [34] Qin, S., Yang, L., Gao, H., Chen, S., Luo, W. "不同应力路径下绢云母片岩粗粒料力学特性试验研究" (Experimental study of mechanical properties of coarse aggregates of sericite schist under different stress paths), *Chinese Journal of Rock Mechanics and Engineering*, 33(9), pp. 1932–1938, 2014. (in Chinese)
- [35] Liu, D., Liu, J., Kong, X., Zou, D. "筑坝堆石料邓肯-张模型参数确定方法的改进" (An improved method to determine Duncan-Zhang model parameters of rockfill material), *Journal of Water Resources and Architectural Engineering*, 14(3), pp. 91–95, 2016. (in Chinese)
- [36] Ling, H., Fu, H., Han, H. Q. "澜沧江如美水电站300m级心墙堆石坝堆石料工程特性试验报告" (Test report on the engineering characteristics of rockfill materials for the 300m core rockfill dam of the Rumei Hydropower Station on the Lancang River), Nanjing Hydraulic Research Institute, Nanjing, China, 2016. (in Chinese)